This article has been accepted for publication in IEEE Transactions on Biomedical Engineering. This is the author's version which has not been fully edited and content may change prior to final publication. Citation information: DOI 10.1109/TBME.2026.3702361

Causal Decomposition of PPG Signals for Cuffless Blood Pressure Estimation

Xinyue Song, Deqi Chen, Andrew Lowe, Zhizhong Fu, Xiaoping Chen, Xiaorong Ding*

***Abstract*— *Objective:* While photoplethysmogram (PPG) signals are physiologically linked to cardiac activity and widely used for cuffless blood pressure (BP) estimation, their correlation with BP remains limited in reliability due to inter-individual heterogeneity. This study aims to isolate the PPG components that have a strong causal relationship with BP, and leverage them to construct reliable cuffless BP estimation models. *Methods:* We propose a causal decomposition framework combining ensemble empirical mode decomposition (EEMD) with counterfactual inference to isolate physiologically causal components in PPG signals. First, PPG signals are adaptively decomposed into multi-scale intrinsic mode functions (IMFs) via EEMD. Then counterfactual PPG sequences are generated through sequentially excluding each IMF, and their causal relationships with BP are quantified via structure causal modeling to identify hemodynamically significant components. Subsequently, robust cuffless BP estimation models are constructed by selectively incorporating components demonstrating strong causal effects. To validate the framework, we benchmark our causality-based models against conventional approaches: pulse arrival time (PAT)-based physiological model, gradient-boosted regression tree (GBRT)-based feature model, and convolutional neural network (CNN)-based time-series model. *Result:* mid-frequency PPG components (IMF4-6) showed strongest BP causality, with CNN model achieving superior estimation performance over PAT and GBRT when utilizing these components. Using IMF45 components, the CNN model achieved BP estimation mean absolute errors of 5.55/3.45 mmHg (systolic/diastolic BP), improving accuracy by 26.39%/17.86% over original PPG. *Conclusion:* Specific PPG frequency bands exhibit physiologically meaningful causal BP relationships. Our causality-driven approach enhances both accuracy and interpretability in cuffless BP estimation. *Significance*： This work establishes a theoretical framework for causal feature selection in BP estimation, and a novel paradigm for physiological signal analysis through causal decomposition.**

***Index Terms*—photoplethysmogram, cuffless blood pressure estimation, causal decomposition, counterfactual inference.**

I. Introduction

PHOTOPLETHYSMOGRAM (PPG) is a biomedical signal acquired through non-invasive optical sensing that detects dynamic changes in blood volume within the subcutaneous microcirculatory system [1]. Its basic principle is to utilize the periodic changes in light absorption by hemoglobin in the blood when a specific wavelength penetrates the skin tissue, thus reflecting the fluctuation of blood volume caused by vascular pulsation [2]. PPG signals contain a wealth of hemodynamic information, such as heart rate (HR), vascular elasticity, and the state of peripheral circulation, making them widely applicable in wearable devices and clinical monitoring [3]. In recent years, PPG-based blood pressure (BP) measurement techniques have attracted significant attention due to their convenience and continuity [4]. Traditional BP measurement relies on cuff-based sphygmomanometers, but their invasiveness and intermittent nature limit real-time monitoring feasibility. In contrast, PPG offers a novel approach for achieving continuous, non-invasive BP monitoring by analyzing the potential correlation between pulse wave morphology and BP.

The relationship between PPG signals and BP stems from the physiological coupling mechanisms of the cardiovascular system. Changes in BP directly affect arterial vasodilation and constriction, thereby altering blood flow velocity and vascular wall tension [5]. These dynamic characteristics are reflected in PPG signals through pulse wave propagation properties, such as waveform rise time and peak-to-peak intervals. The Moens-Korteweg equation [6] establishes a direct relationship between pulse wave velocity (PWV) and the elastic modulus of blood vessels based on the biomechanical properties of the vascular wall, while the Bramwell-Hill equation [7] further establishes the relationship between PWV and arterial compliance. Together, these equations derive an inverse correlation between pulse arrival time (PAT) and BP. Multiple studies have empirically confirmed the PAT-BP relationship using real-world data [8]–[10], and growing evidence suggests that combining PAT with other physiological parameters can improve the accuracy and robustness of BP estimation models

This work was supported in part by Huzhou S&T Special Program of Huzhou (2023GZ01), and in part by National Natural Science Foundation of China (82102178). Asterisk indicates corresponding author.

Xinyue Song, Deqi Chen and Zhizhong Fu are with the School of Life Science and Technology, University of Electronic Science and Technology of China, Sichuan, China.

Andrew Lowe is with the Institute of Biomedical Technologies, Auckland University of Technology, New Zealand.

Xiaoping Chen is with Department of Cardiology, West China Hospital, Sichuan University, Chengdu 610041, China.

Xiaorong Ding is with School of Life Science and Technology, University of Electronic Science and Technology of China, and also with Yangtze Delta Region Institute (Huzhou), University of Electronic Science and Technology of China (e-mail: xiaorong.ding@uestc.edu.cn).

Authorized licensed use limited to: Auckland University of Technology. Downloaded on November 25,2026 at 22:41:49 UTC from IEEE Xplore. Restrictions apply.
© 2026 IEEE. All rights reserved, including rights for text and data mining and training of artificial intelligence and similar technologies. Personal use is permitted, but republication/redistribution requires IEEE permission. See https://www.ieee.org/publications/rights/index.html for more information.

This article has been accepted for publication in IEEE Transactions on Biomedical Engineering. This is the author's version which has not been fully edited and content may change prior to final publication. Citation information: DOI 10.1109/TBME.2026.3702361

[11]–[13]. Additionally, since PPG waveform morphology (e.g., rising slope, dicrotic notch position) correlates with hemodynamic parameters such as vascular elasticity and peripheral resistance, some studies have explored BP estimation through pulse wave analysis. For instance, Ibtehaz *et al.* [14] proposed PPG2ABP, a deep learning-based two-stage cascaded network that analyzes PPG waveforms to estimate continuous arterial BP (ABP) and subsequently predict BP values.

Despite the potential of PPG in BP monitoring, its practical application still faces significant challenges. One is the signal variation caused by individual physiological differences (such as vascular elasticity). The other is that the existing models rely more on statistical correlation than on causal mechanism analysis, which leads to limited generalization ability. A more fundamental issue lies in the composite nature of PPG signals, which represent a mixture of various physiological processes including cardiac pulsation, respiratory modulation, and vascular autoregulation [15]. Conventional PPG based BP estimation methods fail to differentiate the distinct contributions of different frequency components to BP, potentially introducing irrelevant noise or omitting critical information. For instance, high-frequency noise may obscure BP-related low-frequency oscillations. Wu *et al.* [16] used ensemble empirical mode decomposition (EEMD) to decompose the PPG signal into 8 intrinsic mode functions (IMFs), revealing that IMF1-3 could be classified as high-frequency noise caused by mechanical interference, IMF5 contained the effective signal of the diastolic peak, IMF6 reflected heart rate-related arterial pulsations, IMF7 (approximately 0.2 Hz) was associated with respiratory movement, and IMF8 (<0.1 Hz) likely originated from vasomotor activity. Similarly, Hadiyoso e*t al.* [17] compared the empirical mode decomposition (EMD), EEMD, and variational mode decomposition (VMD) methods, finding that IMF7 derived from EEMD most effectively represented the respiratory rate. These studies indicate that the PPG signals from different frequency bands may have varying degrees of correlation with BP. Therefore, identifying causal interactions at specific frequencies is crucial for understanding the underlying mechanisms between PPG and BP. Unlike Hadiyoso e*t al.* [17], which focuses on extracting a single physiological parameter such as respiratory rate using signal decomposition, this study aims to systematically reveal the causal association between different PPG frequency components and BP. Traditional frequency-band analysis has primarily been confined to correlation studies, whereas causal decomposition methods can reveal the directional influence relationship between different frequency components of PPG and BP. Based on the principle of covariation, Yang *et al.* [18]. proposed a causal decomposition approach. Specifically, for two causal signals A and B, if removing a subcomponent of B that is causally related to A leads to a reduction in the instantaneous phase dependence between the two signals, it can be inferred that B exerts a causal influence on A. This study makes a key advance on the causal framework of Yang *et al.* [18]: it innovatively introduces counterfactual reasoning theory and constructs counterfactual sequence analysis to quantify causal effects more rigorously. This integration of methods enhances the depth and robustness of the analysis of the intrinsic causal mechanism of PPG-BP.

In general, this study introduces a novel causal decomposition method, which employs EEMD to decompose PPG signals into distinct frequency components. By integrating counterfactual inference theory, the framework constructs counterfactual sequence analysis to investigate the causal relationships between these PPG frequency components and BP.

The core contribution of this study is that by integrating counterfactual reasoning and causal decomposition, we not only identify the feature frequency bands that are strongly causally associated with BP [19], but also further verify the practical utility of this causal component to improve the performance of cuffless BP estimation models. This work goes beyond the simple causal relationship identification, and provides a key theoretical basis and method support for the realization of high generalization of cuffless BP monitoring.

II. Material

This study utilized publicly accessible data from VitalDB, an open-source repository containing intraoperative physiological signals collected through clinical monitoring systems [19]. Since the dataset is anonymized and freely available, ethical approval was not necessary, and no competing interests were declared. Among the available records, 164 cases with simultaneous ABP, PPG, and lead II electrocardiogram (ECG) waveforms were extracted, comprising 104 male and 60 female participants aged 6–85 years (mean ± SD: 54.8 ± 17.0). All signals were recorded at 500 Hz. In this study, the peaks and troughs of the ABP waveform from each sample were extracted as reference values for SBP and DBP, respectively. A total of 132,354 cardiac cycles were obtained, with the overall distribution illustrated in Fig. 1. The overall mean and standard deviation of SBP were 120.00 ± 17.23 mmHg, while those of DBP were 60.34 ± 13.04 mmHg.

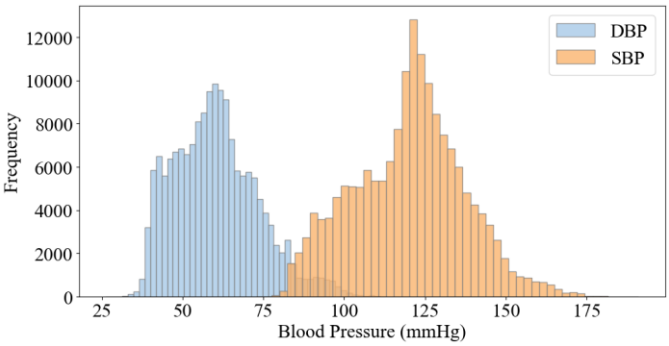


Fig. 1. Distribution of reference BP in the dataset.

III. Method

The overall framework of this study is illustrated in Fig. 2. The research process consists of two main phases. First, causal decomposition is performed to screen IMF components exhibiting strong causal relationships with BP. Subsequently, these selected IMFs are utilized to construct cuffless BP

Authorized licensed use limited to: Auckland University of Technology. Downloaded on November 25,2026 at 22:41:49 UTC from IEEE Xplore. Restrictions apply.
© 2026 IEEE. All rights reserved, including rights for text and data mining and training of artificial intelligence and similar technologies. Personal use is permitted, but republication/redistribution requires IEEE permission. See https://www.ieee.org/publications/rights/index.html for more information.

This article has been accepted for publication in IEEE Transactions on Biomedical Engineering. This is the author's version which has not been fully edited and content may change prior to final publication. Citation information: DOI 10.1109/TBME.2026.3702361

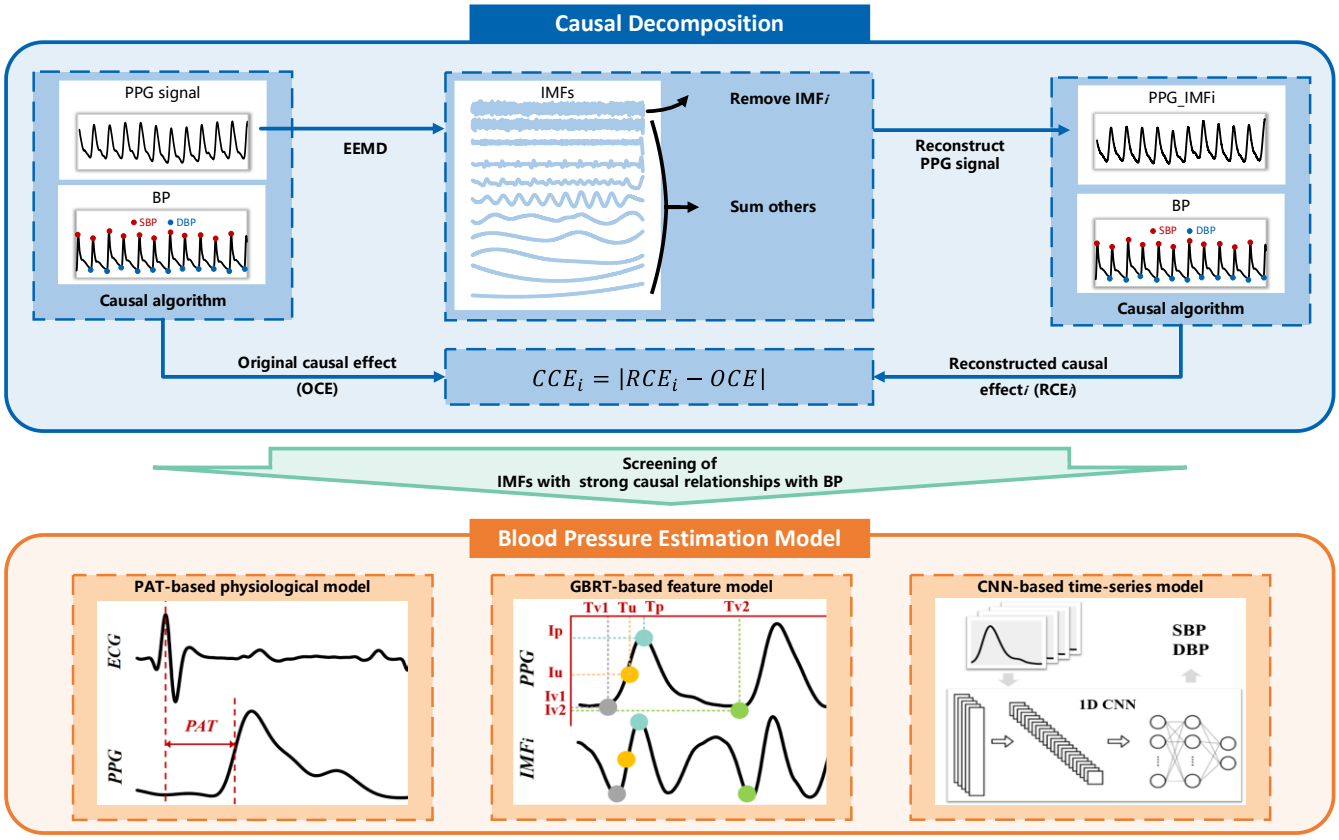


Fig. 2. The overall framework diagram of the proposed study. The PPG is first decomposed into intrinsic mode functions (IMFs) using ensemble empirical mode decomposition (EEMD). By iteratively removing each IMF and reconstructing counterfactual PPG signals, we compute the change of causal effect (CCE) between original PPG–BP (OCE) and counterfactual PPG–BP pairs (RCE). The identified IMFs which exhibit strong causal associations with BP are then used to build three cuffless BP estimation models: (1) pulse arrivaltime (PAT)-based physiological model, (2) gradient-boosted regression tree (GBRT)-based feature model, and (3) convolutional neural network (CNN)-based time-series model.

estimation models across three dimensions: PAT-based physiological model, gradient boosting regression tree (GBRT)-based feature model, and convolutional neural network (CNN)-based time-series model.

A. Causal Decomposition

The proposed causal decomposition method is used for exploring the degree of causal contribution of each subcomponent of PPG to BP. Specifically, three steps are required: *i)* decompose the PPG signal into a set of IMFs using EEMD; *ii)* remove a particular IMF component to construct a counterfactual PPG sequence; and *iii)* compute the causal effects of the original PPG and the counterfactual PPG sequences in relation to the BP. Each step is briefly described in detail below:

1) EEMD

As for the extraction process of IMF in EEMD, the basic steps are as follows: First, the Gaussian white noise with specific amplitude is added to the original signal many times, and the noisy signal is decomposed by EMD each time to obtain a group of IMFs. Then, the corresponding IMFs obtained by each decomposition are ensemble averaged to cancel the noise effect, and finally the EEMD decomposition result is obtained. For EEMD analysis, both the noise level r and the number of ensemble members k affect the bias of the EEMD. A too small r will result in the added noise being ineffective and unable to alleviate modal aliasing, while a too large r will cause the noise to drown out the real signal, leading to decomposition distortion. As for the selection of k, a too small k will retain noise and lead to modal instability, while a too large k will result in excessively high computational costs. To enable EEMD to effectively separate signals of different lengths, this study designs an adaptive rule for the selection of k and r parameters. For r, the noise amplitude is made to adapt to the energy of the signal itself, avoiding excessive perturbation or under-perturbation for high/low energy signals. The calculation formula is:

$$r = \alpha \cdot \frac{std(x_{1:N})}{\sqrt{\frac{1}{N}\sum_{i=1}^{N} x_i^2}} \tag{1}$$

where α is an empirical scaling factor used to balance the perturbation strength of the noise. For k, its selection depends on the signal-to-noise ratio (SNR). In this study, a hierarchical strategy is adopted for the selection of k to achieve a balance between computational efficiency and decomposition fidelity, thereby avoiding the computational burden of uniformly applying a high k value to all signals. The SNR is estimated as:

$$\mathrm{SNR} = 10log_{10}\left(\frac{Var(x_{1:N})}{r^2}\right) \tag{2}$$

Authorized licensed use limited to: Auckland University of Technology. Downloaded on November 25,2026 at 22:41:49 UTC from IEEE Xplore. Restrictions apply.
© 2026 IEEE. All rights reserved, including rights for text and data mining and training of artificial intelligence and similar technologies. Personal use is permitted, but republication/redistribution requires IEEE permission. See https://www.ieee.org/publications/rights/index.html for more information.

This article has been accepted for publication in IEEE Transactions on Biomedical Engineering. This is the author's version which has not been fully edited and content may change prior to final publication. Citation information: DOI 10.1109/TBME.2026.3702361

where $Var(x)$ is the signal variance and r^2 represents the noise energy. The level of k is categorized into three classes based on the estimated value of SNR:

$$k = \begin{cases} 50, & SNR > 20dB \\ 100, & 10dB < SNR \leq 20dB \\ 200, & SNR \leq 10dB \end{cases} \quad (3)$$

As for the setting of the number of IMFs n for the EEMD decomposition, we chose an appropriate value, n= 10, based on the established practice in the literature [17] and through the decomposition stability assessment of the signal subset.

2) Reconstruct Counterfactual PPG Series

The principle of counterfactual theory is to hypothesize changes in conditions based on existing facts to infer possible outcomes, a process that can help better understand causal relationships. After EEMD decomposition, the original signal can be reconstructed by summing all IMF components and the residual term. Therefore, in this study, the actual PPG can be expressed as:

$$PPG(t) = \sum_{k=1}^{n=10} IMF_k(t) + R(t) \quad (4)$$

where *R(t)* is the residual term after decomposition. In order to analyze the causal influence of the components of PPG on BP, the specific component IMF_k in the real PPG is sequentially removed to obtain the counterfactual PPG sequence $PPG_{_IMF_i}$ which has the following expression:

$$PPG_{_IMF_i}(t) = \sum_{k=1}^{n \neq i} IMF_k(t) + R(t) \quad (5)$$

3) Quantifying Causal Effect

Causal effect is the extent to which a cause variable influences another outcome variable in a causal relationship. Direct Linear Non-Gaussian Structural Equation Model (DirectLiNGAM) is an algorithm for causality discovery, which is mainly used to infer the causal structure and causal strength between variables from observed data. The main steps of DirectLiNGAM are to first identify the variables using entropy-based metrics, then determine the causal order of the variables through stepwise regression and independent tests, and finally construct the causal matrix B, where the element b_{ij} denotes the causality of the variable x_j to the variable x_i.

According to the definition of causal decomposition "*cause is that which put, the effect follows; and removed, the effect is removed*" [18], by calculating the difference between the causal effect between the original PPG and ABP and the causal effect between the counterfactual PPG and ABP, i.e. change in causal effect (CCE), the degree of causal influence of each frequency component of PPG on ABP can be quantified. The calculation procedure of CEE is shown in Fig.2. A larger value of CCE_i indicates that the IMF_i obtained by PPG decomposition has a stronger causal effect on ABP.

B. Cuffless Blood Pressure Estimation Using Causality

Causal relationships play a crucial role in variable correlation analysis and prediction. From an information-theoretic perspective, if a unidirectional causality A→B exists, the observed values of B can partially decode the information entropy of A, providing a theoretical foundation for inversely estimating A from B. In cuffless BP prediction, the PPG signal, as a representation of blood volume changes, may have certain IMFs that are directly linked to the dynamic variations of ABP through physiological mechanisms. Selecting components based on causality can effectively eliminate non-causal interference and focus on key physiological features such as vascular tension. This study directly employs the PPG components that exhibit significant causal relationships with ABP for BP estimation, thereby validating the conclusions drawn from causal discovery.

To thoroughly validate the effectiveness of causal components, this study designed three types of models: PAT-based physiological model, GBRT-based feature model, and CNN-based time-series model. The detailed descriptions of each model are as follows:

1) PAT-based physiological model

Physiological models serve as the foundational framework for cuffless BP estimation, with their core advantages lying in strong interpretability and physiology-driven mechanisms. These models establish physical relationship equations between pulse transit time (PAT) and BP, thereby directly reflecting the influence of hemodynamic parameters on BP. This study adopts the classical cuffless BP estimation physiological model proposed by Proença *et al.*[20]:

$$BP = alnPTT + b \quad (6)$$

Where PAT is defined as the time interval between the maximum upslope point of the PPG waveform and the peak of the corresponding ECG R-wave within a cardiac cycle. For each sample, the first three data points are selected as calibration points to estimate systolic BP (SBP) and diastolic BP (DBP) individually.

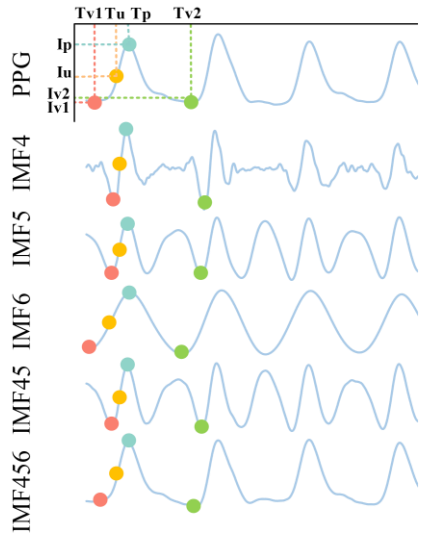


Fig. 3. Schematic diagram of feature extraction for photoplethysmogram (PPG) intrinsic mode functions (IMFs). Four fiducial points are identified: the onset of the cardiac cycle (Red dot, (Tv1, Iv1)), the maximum upslope point (Yellow dot, (Tu, Iu)), the peak (Blue dot, (Tp, Ip)), and the end of the cardiac cycle (Green dot, (Tv2, Iv2)).

Authorized licensed use limited to: Auckland University of Technology. Downloaded on November 25,2026 at 22:41:49 UTC from IEEE Xplore. Restrictions apply.
© 2026 IEEE. All rights reserved, including rights for text and data mining and training of artificial intelligence and similar technologies. Personal use is permitted, but republication/redistribution requires IEEE permission. See https://www.ieee.org/publications/rights/index.html for more information.

This article has been accepted for publication in IEEE Transactions on Biomedical Engineering. This is the author's version which has not been fully edited and content may change prior to final publication. Citation information: DOI 10.1109/TBME.2026.3702361

TABLE I
FEATURE DEFINITION FOR EACH PPG IMF

No.	Feature Name	Definition
1	PAT	Time difference between the maximum upslope of the PPG waveform and the R-peak of the ECG
2	I_{v1}	Intensity at the onset point of the PPG
3	I_p	Intensity at the systolic peak of the PPG
4	AA	Amplitude difference between the onset and systolic peak（$I_P - I_{v1}$）
5	TD	Time difference from onset to systolic peak（$T_P - T_{v1}$）
6	RRI	Time interval of each cardiac cycle（$T_{v2} - T_{v1}$）
7	SDR	Ratio of systolic duration to diastolic duration（$\frac{TD}{RRI-TD}$）
8	STT	Inverse of the peak of the first derivative of the PPG waveform
9	SYM	Symmetry measure
10	S1	Integral of the PPG waveform area from onset to systolic peak
11	S2	Integral of the PPG waveform area from systolic peak to end point

2) *Feature-based Model*

By extracting features from IMFs of the PPG signal, a machine learning-based cuffless BP estimation model can be constructed to further capture nonlinear characteristics embedded in the PPG waveform. This approach enables the quantitative assessment of contributions from different physiological factors and causal relationships to BP estimation. As illustrated in Fig. 3, the extracted features in this study were derived by identifying common fiducial points across several IMFs. Based on each fiducial point's intensity (I) and temporal location (T), a total of 11 shared features were computed. The precise definitions of these features are detailed in Table I.

This study employs the gradient boosting regression tree (GBRT) as the feature modeling approach. GBRT is an iterative decision tree algorithm that constructs an ensemble model by combining multiple decision trees, where each new tree minimizes the prediction residuals of the existing base model, and the final estimation is obtained by accumulating the outputs of all trees [21]. To reduce randomness caused by a single division of the training set, 10-fold cross-validation was adopted with subject-based dataset partitioning. Based on preliminary experimental results, the hyperparameters of GBRT were set as follows: the maximum number of iterations was set to 300, the maximum tree depth was set to 6, and the learning rate was 0.05.

3) *Time Series Model*

By directly conducting deep learning modeling and analysis on the time series of IMFs of PPG, the rich time and frequency domain information related to BP contained in it is explored more comprehensively, and the IMF sequence is directly mapped to the BP value. The architecture of the proposed time series model is illustrated in Fig. 4. First, all component sequences are divided into single cycles by identifying the starting and ending points of each cardiac cycle. Then, cubic spline interpolation is used to resample all single-cycle sequences to 500 points uniformly, followed by normalization to eliminate amplitude differences between PPG and IMF components. For each subject, the data is divided into training set (first 60% of cycles), validation set (middle 20% of cycles), and test set (last 20% of cycles) in chronological order. This partitioning method maintains the continuity of time series while preventing future information leakage. SmoothL1Loss [22] is selected as the loss function. To prevent overfitting during training across different subjects, a dropout layer is added between the fully connected layer and output layer. The AdamW optimizer (initial learning rate=0.001, weight decay=3×10^{-4}) is employed for training. The model uses a batch size of 64 and runs for 50 epochs, combined with early stopping strategy to monitor validation loss for improved generalization capability.

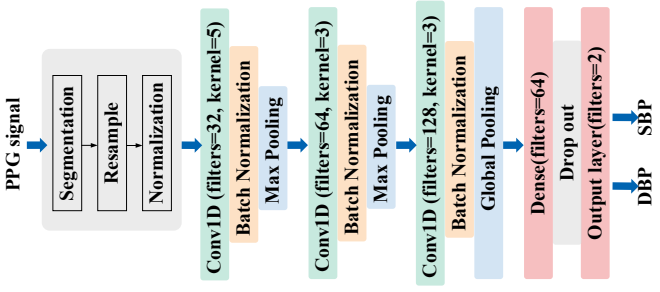


Fig. 4. Schematic diagram of the CNN-based time series model for cuffless blood pressure (BP) estimation.

IV. Result

A. *Result of Causal Decomposition*

The waveforms of the IMFs obtained through EEMD decomposition are shown in Fig. 5 (a). By sequentially removing each IMF component and reconstructing the PPG counterfactual sequences, a total of 10 counterfactual sequences were generated, whose waveforms are presented in Fig. 5 (b). The causal effect analysis results between the original PPG sequence and the counterfactual PPG sequences with the ABP sequence are shown in Fig. 6. This analysis, conducted on the entire 164 samples, aims to verify whether there exists a

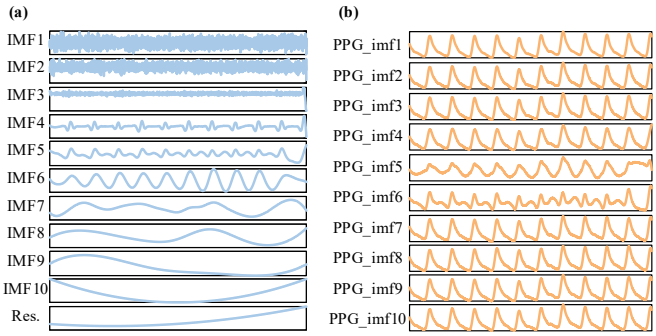


Fig. 5. Waveform plot of causal decomposition: (a) ten IMFs and residuals (Res.) of PPG via EEMD; (b) corresponding reconstructed counterfactual PPG sequences (PPG_imf1 – PPG_imf10).

Authorized licensed use limited to: Auckland University of Technology. Downloaded on November 25,2026 at 22:41:49 UTC from IEEE Xplore. Restrictions apply.
© 2026 IEEE. All rights reserved, including rights for text and data mining and training of artificial intelligence and similar technologies. Personal use is permitted, but republication/redistribution requires IEEE permission. See https://www.ieee.org/publications/rights/index.html for more information.

This article has been accepted for publication in IEEE Transactions on Biomedical Engineering. This is the author's version which has not been fully edited and content may change prior to final publication. Citation information: DOI 10.1109/TBME.2026.3702361

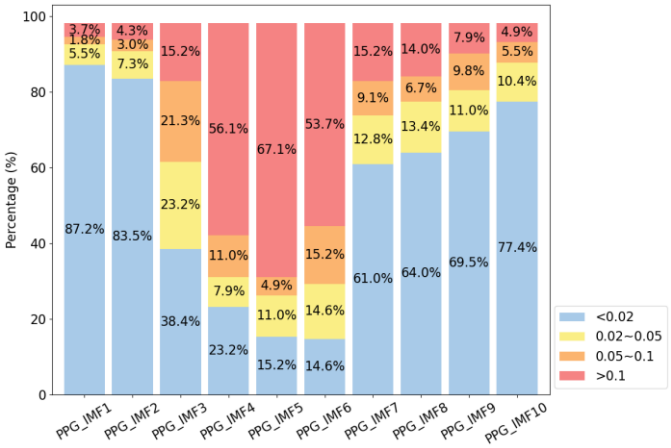


Fig. 6. 100% stacked plot of changes in causal effect (CCE) for each reconstruction PPG sequence and arterial blood pressure (ABP), categorized by CCE strength levels (color-coded).

TABLE II
STATISTICAL ANALYSIS OF CAUSAL DIRECTIONALITY BETWEEN PHYOTOPLETHYSMOGRAM (PPG), ITS INTRINSIC MODE FUNCTION (IMFS) AND ARTERIAL BLOOD PRESSRUE (ABP)

Causal direction	PPG →ABP	ABP → PPG	No causality
PPG	**28.1%**	**70.0%**	**1.9%**
PPG_{-IMF1}	28.8%	69.4%	1.9%
PPG_{-IMF2}	28.1%	70.0%	1.9%
PPG_{-IMF3}	28.1%	62.5%	3.1%
$\boldsymbol{PPG_{-IMF4}}$	**33.8%**	**62.5%**	**3.8%**
$\boldsymbol{PPG_{-IMF5}}$	**35.6%**	**59.4%**	**5.0%**
$\boldsymbol{PPG_{-IMF6}}$	**16.3%**	**77.5%**	**6.3%**
PPG_{-IMF7}	26.9%	71.3%	1.9%
PPG_{-IMF8}	28.1%	70.0%	1.9%
PPG_{-IMF9}	29.4%	68.8%	1.9%
PPG_{-IMF10}	29.4%	68.8%	1.9%

universal and stable pattern of causal association between different IMF components and ABP, thereby providing a theoretical basis for feature selection in subsequent model construction. A 100% stacked column chart was used to visually display the overall variation in causal strength across all samples. For IMF1, IMF2, IMF3, IMF8, IMF9, and IMF10, over 80% of the samples had a CCE $\leqslant$ 0.1, indicating that these components generally had almost no effect on ABP. In contrast, for IMF4, IMF5, and IMF6, more than 50% of the samples exhibited CCE > 0.1. Among these, IMF5 showed the most significant variation in causal strength, with 67.1%, 4.9%, 11.0% and 15.2% of the samples falling into the CCE > 0.1, 0.05 < CCE < 0.1, 0.02 < CCE < 0.05 and CCE $<$ 0.02 ranges, respectively. Table II summarizes the causal directions between the original PPG sequence, the counterfactual PPG sequences, and ABP. For the original PPG, it can be observed that 70% of the samples exhibit the causal direction ABP→PPG, indicating that the original PPG acts as a result of ABP, and it is feasible to inversely estimate BP using the original PPG.

For the counterfactual PPG sequences, the results show that IMF4 and IMF5 exhibit a significant reduction in the number of samples with the ABP→PPG causal direction across all samples. This suggests that after removing IMF4 or IMF5 from the original PPG, the causal relationship with ABP reverses in some samples, further confirming that IMF4 and IMF5 have a strong causal influence on ABP. The case of IMF6 differs from the other components. In some samples, removing the IMF6 component changes the causal direction from PPG→ABP to ABP→PPG, while in more samples, the removal of IMF6 results in no causal relationship with ABP.

B. Result of Cuffless Blood Pressure Estimation

Based on the causal decomposition results, this study selected IMF4, IMF5, and IMF6 of the PPG for cuffless BP estimation and combined them to generate IMF45 and IMF456 sequences to enhance model performance. Among these, IMF4 and IMF5 exhibit a significant causal relationship with ABP, serving as the core basis for modeling, while IMF6, despite its weaker causality, provides supplementary physiological information that effectively enhances BP estimation. By integrating multiple components, the model can more comprehensively capture physiological features, thereby improving the accuracy and robustness of BP estimation. Additionally, this study employed three types of models to estimate BP using the original PPG signal. The effect of BP estimation between the original PPG model and the causal component model was compared.

Fig. 7 presents the performance of three distinct models for BP prediction using PPG components that exhibit high causal relevance to BP, with MAE ± SD used as the accuracy metric. The three subplots should be interpreted independently: Fig. 7(a) corresponds to the PTT model, Fig. 7(b) to the GBRT model, and Fig. 7(c) to the CNN model. The overall trend indicates that all models achieve consistently higher prediction accuracy when using the causal component IMF45 compared to using the original PPG signal. For SBP estimation, the accuracies of the PAT-based physiological model, GBRT-based feature model, and CNN-based model using IMF45 were 8.81mmHg, 6.43mmHg, and 5.55mmHg, respectively. Similarly, for DBP estimation, the corresponding accuracies were 5.08mmHg, 4.61mmHg, and 3.45mmHg. Furthermore, when other causal components besides IMF45 were used for BP estimation, the accuracy was consistently higher than that achieved with the original PPG signal. This indicates that while the original PPG signal provides some BP estimation capability, its precision and stability are limited due to the inclusion of various noise and interference components. In contrast, the PPG component based on causal screening is able to capture blood pressure related information more effectively, and this advantage is verified in different types of models.

Additionally, this study employs the internationally recognized standard for BP measurement, namely the British Hypertension Society (BHS) [23] protocol, to evaluate the accuracy of the models. Table III presents the detailed grade classification of the BHS standards and the results of BP estimation using the original PPG and the IMF45 component of PPG by the three models in this study. Overall, all three models exhibit slight improvements in BP prediction accuracy grades

Authorized licensed use limited to: Auckland University of Technology. Downloaded on November 25,2026 at 22:41:49 UTC from IEEE Xplore. Restrictions apply.
© 2026 IEEE. All rights reserved, including rights for text and data mining and training of artificial intelligence and similar technologies. Personal use is permitted, but republication/redistribution requires IEEE permission. See https://www.ieee.org/publications/rights/index.html for more information.

This article has been accepted for publication in IEEE Transactions on Biomedical Engineering. This is the author's version which has not been fully edited and content may change prior to final publication. Citation information: DOI 10.1109/TBME.2026.3702361

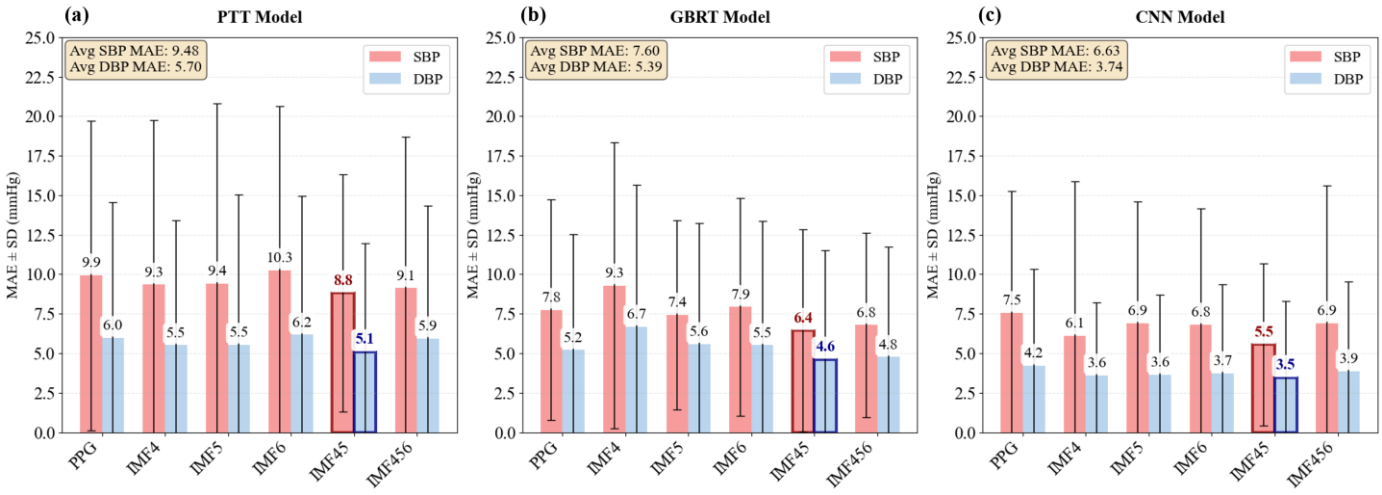


Fig. 7. The accuracy of the three models in estimating systolic blood pressure (SBP) (red) and diastolic BP (DBP) using the original PPG and different IMFs: (a) pulse transit time (PTT) Model; (b) gradient boosting regression tree (GBRT) model; (c) convolutional neural network (CNN) model.

TABLE III
ACCURACY OF BLOOD PRESSURE ESTIMATION UNDER BHS STANDARD

			≤5 mmHG	≤10 mmHG	≤15 mmHG	Grade
BHS			60%	85%	95%	A
			50%	75%	90%	B
			40%	65%	85%	C
PAT Model	Original PPG	SBP	35.34%	62.49%	79.63%	D
		DBP	56.03%	83.41%	93.28	B
	PPG IMF45	SBP	38.02%	63.88%	81.77%	D
		DBP	61.51%	87.13%	96.27%	A
GBRT	Original PPG	SBP	44.44%	71.78%	86.39%	C
		DBP	62.22%	85.88%	94.38%	B
	PPG IMF45	SBP	53.28%	79.23%	90.62%	B
		DBP	65.92%	87.19%	94.81%	B
CNN	Original PPG	SBP	51.94%	75.87%	85.59%	C
		DBP	71.83%	90.66%	97.24%	A
	PPG IMF45	SBP	57.40%	84.61%	94.19%	B
		DBP	77.33%	93.94%	99.18%	A

when using IMF45 for estimation compared to the original PPG with the estimation grades for DBP being higher than those for SBP. The PAT model achieves BHS grades D and A for SBP and DBP estimation, respectively, when using IMF45. The GBRT model attains BHS grade B for both SBP and DBP estimation with IMF45, while the CNN model reaches BHS grades B and A for SBP and DBP estimation, respectively, using IMF45.

Furthermore, this study evaluates the accuracy of BP estimation using each causal component according to the ACC/AHA HTN BP classification criteria [24], thereby validating the clinical applicability of the models across different BP ranges, with particular focus on their performance in hypertensive stages. Table IV presents a comparison of the predictive performance of the CNN model using the original

TABLE IV
COMPARISON OF THE ACCURACY OF BLOOD PRESSURE ESTIMATION BY CNN USING THE ORIGINAL PPG AND IMF45 UNDER DIFFERENT BLOOD PRESSURE LEVELS

BP Ranges	PPG Compone-nts	SBP (mmHg)		DBP (mmHg)	
		ME±SD	MAE	ME±SD	MAE
Normal (n=16995)	$PPG_{original}$	0.29±8.58	5.81	-0.29±4.30	3.11
	PPG_{IMF45}	**1.70±6.75**	**4.98**	**0.34±4.55**	**3.21**
Elevated (n=6933)	$PPG_{original}$	-6.30±9.06	8.53	-2.30±4.39	3.80
	PPG_{IMF45}	**-4.41±7.90**	**6.44**	**-1.42±3.96**	**3.02**
Stage 1 hypertension (n=5360)	$PPG_{original}$	-5.88±9.30	8.53	-3.96±6.04	5.46
	PPG_{IMF45}	**-4.95±8.79**	**7.26**	**-3.04±5.66**	**4.53**
Stage 2 hypertension (n=3002)	$PPG_{original}$	-9.19±11.17	10.65	-4.62±8.41	5.77
	PPG_{IMF45}	**-7.09±10.62**	**7.88**	**-3.54±6.54**	**4.78**

Notes: BP is categorized into 4 levels on the basis of average BP measured in a healthcare setting: Normal 1 (SBP <120 mmHg and DBP <80 mmHg), Elevated (SBP 120-129 mmHg and DBP <80 mmHg), and Stage 1 (SBP 130-139 mmHg or DBP 80-89 mmHg) or Stage 2 hypertension (SBP ≥140 mmHg or DBP ≥90 mmHg) [24].

PPG signal versus the IMF45 component for BP estimation across different BP categories (Normal, Elevated, Stage 1 hypertension, and Stage 2 hypertension) on the test set. Overall, IMF45 demonstrates superior or comparable predictive performance across all BP categories. For SBP and DBP, IMF45 achieves MAE of 4.98 mmHg and 3.21 mmHg, respectively, in the Normal group, slightly outperforming the original PPG. Its advantage becomes more pronounced in the Elevated and hypertensive stages (Stage 1/2), with SBP MAE reductions of 1.3–2.8 mmHg and DBP MAE reductions of 0.8–1.0 mmHg. Additionally, IMF45 exhibits generally smaller standard deviations in prediction errors, indicating higher estimation stability, particularly with reduced systematic bias in hypertensive ranges. For instance, the SD of the DBP estimation in Stage 2 improves from 8.41 mmHg to 6.54 mmHg. These results verify that IMF45 as a causal association feature can more accurately capture the change of BP, especially in the pathological range of BP. To investigate the underlying causes, elevated vascular stiffness and altered PPG waveform morphology in hypertensive patients were considered. The

Authorized licensed use limited to: Auckland University of Technology. Downloaded on November 25,2026 at 22:41:49 UTC from IEEE Xplore. Restrictions apply.
© 2026 IEEE. All rights reserved, including rights for text and data mining and training of artificial intelligence and similar technologies. Personal use is permitted, but republication/redistribution requires IEEE permission. See https://www.ieee.org/publications/rights/index.html for more information.

This article has been accepted for publication in IEEE Transactions on Biomedical Engineering. This is the author's version which has not been fully edited and content may change prior to final publication. Citation information: DOI 10.1109/TBME.2026.3702361

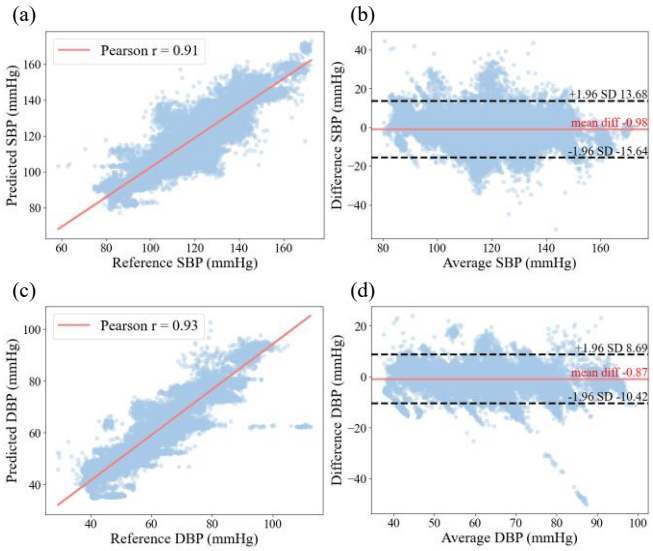


Fig. 8. Distributions of blood pressure and reference blood pressure estimated by the time-series model: (a) Scatterplot of SBP; (b) Bland-Altman plot of SBP; (c) Scatterplot of DBP; (d) Bland-Altman plot of DBP.

original PPG signal is prone to distortion from such morphological changes, leading to significant measurement inaccuracies. In contrast, IMFs extracted by PPG adaptively capture the underlying oscillatory patterns of the cardiovascular system. The IMFs identified as most relevant for causality, IMF4/5, may correspond to physiological oscillations that maintain a more stable relationship with central BP determinants or even peripheral vasculature.

This study further conducted consistency and correlation analyses between the estimated BP values derived from different causal components using the three models and the reference BP values. Due to space limitations, Fig. 8 only SBP and DBP using IMF45.

As shown in the scatter plots of Fig. 8 (a) and Fig. 8 (c), the correlation coefficients between the estimated and reference values for SBP and DBP are 0.91 and 0.93, respectively. The Bland-Altman plots in Fig. 8 (b) and Fig. 8 (d) indicate that most differences for both SBP and DBP fall within the limits of agreement, demonstrating high consistency between the model's estimates and the reference values. However, some outliers are observed, which may be attributed to excessively short continuous PPG cycles in certain samples, leading to overfitting during model training and resulting in significant deviations between predicted and reference values.

C. *Interpretability Analysis*

This study further analyzes the feature significance of the GBRT and CNN two black-box models when predicting BP using different components. By comparing the feature importance between the original PPG signal and the IMF45 composite component, we aim to provide deeper insights into the physiological mechanisms underlying BP estimation.

Fig. 9 presents a comparison of feature importance when the GBRT model estimates SBP/DBP using either the original PPG or IMF45 components. The results demonstrate that: *i)* PAT maintains the highest importance across both input types due to its direct correlation with vascular properties; *ii)* RRI shows

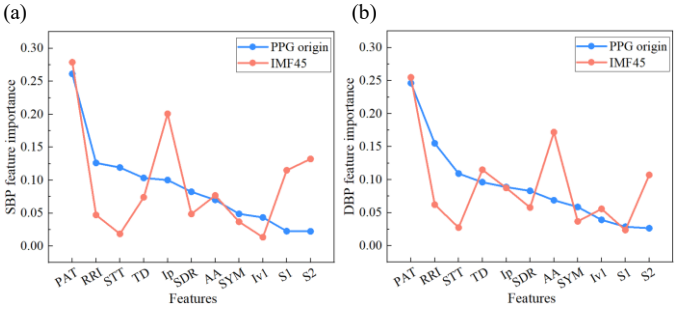


Fig. 9. Ranking of feature importance estimated by feature model when estimating SBP (a) and DBP (b).

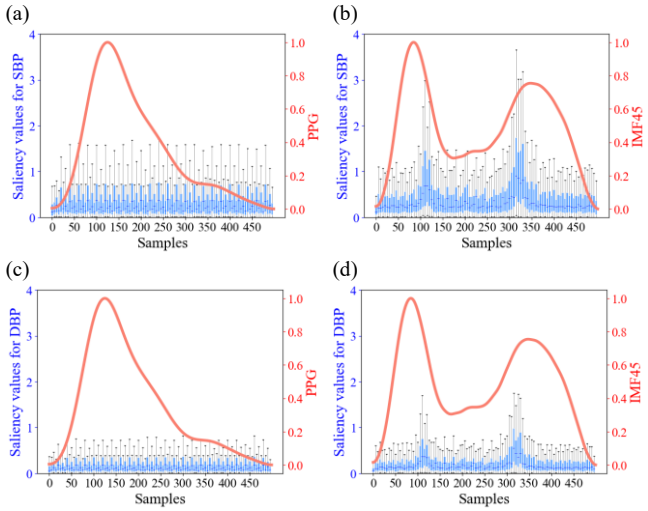


Fig. 10. Waveform significance plot of blood pressure estimated by the time-series model: estimation of SBP using PPG (a); estimation of SBP using IMF45 (b); estimation of DBP using PPG (a); estimation of DBP using IMF45 (b).

relatively high importance with the original PPG but significantly decreases with IMF45; *iii*) STT, Tp and other features exhibit markedly different importance levels between the two inputs, suggesting that IMF45 may reconstruct their physiological representations. These findings provide valuable guidance for optimizing feature combination strategies to enhance estimation accuracy.

Fig. 10 present the saliency maps of original PPG waveforms and IMF45 waveforms when the CNN model estimates SBP and DBP, respectively. Saliency maps serve as a visualization tool for interpreting deep learning model decisions by computing the gradient of model output relative to input data, where the absolute gradient value indicates each data point's sensitivity to model prediction. Higher absolute gradient values signify greater importance of that data point to the model's prediction. In Fig. 10, the red waveforms represent template waveforms of either original PPG or IMF45 signals, obtained by averaging all periodic signals from each subject. Comparative analysis reveals that IMF45 waveforms significantly amplify diastolic fluctuations compared to original PPG. To evaluate waveform significance, this study calculated absolute gradient values for 500 sampling points relative to SBP/DBP predictions, with distributions displayed as blue boxplots in 5-point units. The results demonstrate: *i)* The CNN model exhibits lower sensitivity to DBP than SBP; *ii)* Original

Authorized licensed use limited to: Auckland University of Technology. Downloaded on November 25,2026 at 22:41:49 UTC from IEEE Xplore. Restrictions apply.
© 2026 IEEE. All rights reserved, including rights for text and data mining and training of artificial intelligence and similar technologies. Personal use is permitted, but republication/redistribution requires IEEE permission. See https://www.ieee.org/publications/rights/index.html for more information.

This article has been accepted for publication in IEEE Transactions on Biomedical Engineering. This is the author's version which has not been fully edited and content may change prior to final publication. Citation information: DOI 10.1109/TBME.2026.3702361

PPG shows relatively stable significance distribution, while IMF45 displays markedly higher values at systolic descending slopes and diastolic ascending slopes. This indicates IMF45's enhanced capability to focus on BP-related local features, thereby improving both model performance and interpretability.

V. Discussion

A. Causal Component Selection and Model Superiority

This study integrates counterfactual inference theory with EEMD to establish a causal decomposition framework for PPG signals. By computing causal strength metrics between counterfactual PPG sequences and ABP, we identified that the mid-frequency component IMF5 exhibits the strongest causal association with ABP, significantly surpassing low-frequency components (IMF9-10) and high-frequency components (IMF1-3). This finding provides a novel theoretical perspective for traditional PPG signal analysis—unlike conventional IMF selection criteria based on spectral energy or morphological similarity, our causal decomposition approach precisely identifies physiologically meaningful core components from ten IMFs. The BP estimation model constructed using IMF45 demonstrates superior stability on the VitalDB dataset, with significantly reduced estimation errors compared to the original PPG signal model, thereby validating the effectiveness of our causal component screening methodology.

B. Differential Effects of PPG Frequency Bands on BP

The results of the causal decomposition in this study allow us to interpret the differential mechanisms by which various frequency-band IMF components derived from PPG decomposition affect BP from three perspectives: low, medium, and high frequencies.

The low-frequency components (IMF8-10) are typically associated with physiological regulatory processes such as respiratory rhythms and autonomic nervous system modulation [25]. These components may reflect vascular compliance and hemorheological properties, thereby influencing baseline fluctuations in ABP. Therefore, the causal decomposition results indicate that these low-frequency components have relatively minor effects on ABP.

The medium-frequency components (IMF4-7) exhibit dynamic characteristics highly synchronized with the cardiac cycle. Their physiological mechanisms are likely related to cardiac mechanical activity and vascular wall elasticity [26]. As shown in Fig. 5(a), the medium-frequency component IMF5 displays more distinct diastolic and systolic waveforms compared to the original PPG. Furthermore, the causal decomposition results demonstrate that IMF5 has a stronger causal relationship with ABP than all other components.

The high-frequency components (IMF1-3) are generally associated with signal noise and rapid microvascular changes. These components may reflect local blood flow variations in the microcirculation but have minimal direct impact on ABP. The causal decomposition results confirm that these high-frequency components indeed show weaker causal relationships with ABP.

C. Causal direction of PPG and ABP

The analysis of causal direction between ABP and PPG, as presented in Table II, reveals that the majority of subjects demonstrate a causal influence of ABP→PPG. This phenomenon can be physiologically explained through several mechanisms. First, changes in ABP directly reflect pressure variations in the arterial system during cardiac systole and diastole. These pressure fluctuations propagate through the arterial network to peripheral vessels, consequently modulating both the amplitude and waveform characteristics of PPG signals. Second, the generation mechanism of PPG signals is fundamentally linked to hemorheological properties, for which ABP serves as a primary determinant. This pathophysiological relationship further substantiates the causal pathway whereby ABP variations drive PPG signal changes. The consistent observation of this unidirectional causality across most study participants strongly supports the physiological plausibility of ABP as the causal driver in this relationship.

D. Advantages of causal models

In contrast to traditional correlation-driven cuffless BP estimation methods, causality-based modeling strategies can effectively distinguish between genuine causal features and spurious correlations in PPG signals, thereby significantly improving model stability. For instance, Liu *et al.* [27] proposed CiGNN, a causal inference-based two-stage framework for cuffless BP estimation. By employing causal discovery algorithms to screen 222 non-invasive physiological features, they identified key features causally linked to BP variations and used them for BP estimation, substantially improving continuous BP estimation accuracy. Our team's preliminary research [28] also demonstrated that eliminating the confounding effect of HR on PAT-based BP estimation significantly enhanced the precision of BP regression models. These findings collectively validate the universal value of causal modeling. Moreover, compared to black-box deep learning models, causality-based BP estimation models offer superior interpretability.

Notably, the "causality-frequency domain" dual-screening mechanism proposed in this study demonstrates unique innovation: first decoupling the time-frequency mixed characteristics of PPG signals through EEMD, then eliminating non-causal frequency bands via counterfactual analysis. This causality-based processing strategy endows the model with superior cross-subject generalization capability across datasets.

E. Constraints of traditional IMF approaches

Although EMD-based methods have been previously applied in PPG analysis, existing studies generally suffer from three fundamental limitations. First, the selection of IMFs lacks theoretical justification. For instance, Wu *et al.* [29] directly used IMF4 of PPG to extract features for building an ANN-based cuffless BP estimation model without clarifying the physical relationship between this component and BP. Second, significant interference from high-frequency noise exists. Song *et al.* [30] fed all IMFs into a hybrid LSTM-CNN model for cuffless BP estimation, whereas our causal decomposition

Authorized licensed use limited to: Auckland University of Technology. Downloaded on November 25,2026 at 22:41:49 UTC from IEEE Xplore. Restrictions apply.
© 2026 IEEE. All rights reserved, including rights for text and data mining and training of artificial intelligence and similar technologies. Personal use is permitted, but republication/redistribution requires IEEE permission. See https://www.ieee.org/publications/rights/index.html for more information.

This article has been accepted for publication in IEEE Transactions on Biomedical Engineering. This is the author's version which has not been fully edited and content may change prior to final publication. Citation information: DOI 10.1109/TBME.2026.3702361

results demonstrate that high and low frequency components exhibit weak causal relationships with ABP, thereby introducing interference. Third, the decomposition results of IMFs exhibit randomness, potentially leading to inconsistencies across studies.

To address these issues, this study developed an adaptive EEMD parameter optimization scheme combined with causal-effect-based component selection. This approach ensures that the ultimately selected IMFs possesses reproducible physiological significance. Such a design provides a new paradigm for combining parameter optimization with causal verification for physiological parameter estimation based on signal decomposition.

F. Limitations and Prospects

Although this study has made significant progress in PPG signal causal decomposition and cuffless BP estimation, several limitations warrant further exploration and improvement.

First, the DirectLiNGAM algorithm employed in this study is based on linear causal assumptions, whereas the actual relationship between PPG and ABP is likely to involve significant nonlinear components. This may lead to underestimation of some genuine causal relationships.

Second, although IMF4 and IMF5 of PPG emerged as the most causal components in our population-level approach, the IMFs most causal to ABP for different levels of BP variation in different individuals may be state-dependent and may vary with individual hemodynamic status. Central to our approach is the assumption that PPG-ABP causality is physiologically driven, requiring an ABP signal of high physiological fidelity. To ensure this, we used ABP signals collected via clinical invasive arterial catheters, a standard practice that effectively minimizes measurement noise and provides a high-quality basis for causal inference. Consequently, PPG signals obtained from different devices or under varying measurement conditions may yield divergent distributions of estimated causal effects. This variability must be accounted for in future research. Accordingly, our future work will focus on developing personalized and adaptive causality models capable of dynamically identifying the most relevant IMF components for each individual, while filtering out non-physiological coupling components. Achieving such adaptive and individualized modeling represents a crucial step toward the practical application of this technology in continuous wearable health monitoring devices.

Third, an important limitation of this study is that, constrained by the sample size of the dataset (N=164) and the within-individual BP variability range, the current subject-partitioned model performance does not yet meet the requirements for clinical deployment. This underscores the necessity of future validation in larger cohorts with more dynamic BP variations.

Looking ahead, an end-to-end personalized causal BP estimation framework could be developed: by real-time monitoring of individual PPG-ABP dynamic interactions, automatically identifying the most causally representative IMF components under current physiological states (e.g., enhanced high-frequency components during exercise versus dominant mid-frequency components at rest), and dynamically adjusting model inputs. Such an adaptive mechanism could address challenges posed by individual differences and state dependency, advancing cuffless BP monitoring from population-based models toward personalized medicine.

VI. CONCLUSION

This study adopts a time-series perspective to investigate the causal relationship between PPG components and ABP by analyzing decomposed elements of PPG signals and their association with ABP. The research employs causal decomposition methodology, utilizing EEMD to break down PPG signals into multiple IMFs. Through constructing counterfactual PPG sequences and applying causal discovery algorithms, we quantitatively evaluate the causal strength between each IMF component and ABP. Based on causal decomposition results, we developed three distinct blood pressure estimation models: physiological model, feature-based model, and time-series model. A comprehensive three-dimensional comparison was conducted between models using PPG components with strong causal links to ABP versus those using raw PPG signals. And the evaluation demonstrates that time-series models incorporating causal components exhibit superior performance in cuffless BP estimation. This work addresses the limitations of conventional waveform correlation analysis between PPG and ABP, while providing novel theoretical and technical support for applying PPG components in blood pressure estimation.

REFERENCES

[1] J. Allen, 'Photoplethysmography and its application in clinical physiological measurement', *Physiol. Meas.*, vol. 28, no. 3, pp. R1–R39, Mar. 2007

[2] C. Lee *et al.*, 'Relations between ac-dc components and optical path length in photoplethysmography', *J. Biomed. Opt.*, vol. 16, no. 7, p. 077012, 2011

[3] J.-S. Park *et al.*, 'Relationship between arterial stiffness and variability of home blood pressure monitoring', *Medicine*, vol. 99, no. 30, p. e21227, Jul. 2020

[4] M. Elgendi *et al.*, 'Recommendations for evaluating photoplethysmography-based algorithms for blood pressure assessment', *Commun Med*, vol. 4, no. 1, p. 140, Jul. 2024

[5] X. Ding and Y.-T. Zhang, 'Pulse transit time technique for cuffless unobtrusive blood pressure measurement: from theory to algorithm', *Biomed. Eng. Lett.*, vol. 9, no. 1, pp. 37–52, Feb. 2019

[6] W. Chen *et al.*, 'Continuous estimation of systolic blood pressure using the pulse arrival time and intermittent calibration', *Med. Biol. Eng. Comput.*, vol. 38, no. 5, pp. 569–574, Sep. 2000

[7] J. C. Bramwell and A. V. Hill, 'The velocity of pulse wave in man', *Proceedings of the Royal Society of London. Series B, Containing Papers of a Biological Character*, vol. 93, no. 652, pp. 298–306, 1992

[8] R. Ochiai *et al.*, 'The relationship between modified pulse wave transit time and cardiovascular changes in isoflurane anesthetized dogs', *Journal of Clinical Monitoring and Computing*, vol. 15, no. 7/8, pp. 493–501, 1999

[9] N. R. Gaddum *et al.*, 'A technical assessment of pulse wave velocity algorithms applied to non-invasive arterial waveforms', *Ann Biomed Eng*, vol. 41, no. 12, pp. 2617–2629, Dec. 2013

[10] S. S. Mousavi *et al.*, 'Blood pressure estimation from appropriate and inappropriate PPG signals using A whole-based method', *Biomedical Signal Processing and Control*, vol. 47, pp. 196–206, Jan. 2019

Authorized licensed use limited to: Auckland University of Technology. Downloaded on November 25,2026 at 22:41:49 UTC from IEEE Xplore. Restrictions apply.
© 2026 IEEE. All rights reserved, including rights for text and data mining and training of artificial intelligence and similar technologies. Personal use is permitted, but republication/redistribution requires IEEE permission. See https://www.ieee.org/publications/rights/index.html for more information.

This article has been accepted for publication in IEEE Transactions on Biomedical Engineering. This is the author's version which has not been fully edited and content may change prior to final publication. Citation information: DOI 10.1109/TBME.2026.3702361

[11] Z.-B. Zhou *et al.*, 'Wearable Continuous Blood Pressure Monitoring Devices Based on Pulse Wave Transit Time and Pulse Arrival Time: A Review', *Materials*, vol. 16, no. 6, p. 2133, Mar. 2023
[12] Y. Huang *et al.*, 'Camera-Based Blood Pressure Monitoring Based on Multisite and Multiwavelength Pulse Transit Time Features', *IEEE TRANSACTIONS ON INSTRUMENTATION AND MEASUREMENT*, vol. 73, 2024
[13] G. Slapničar *et al.*, 'Feasibility of Remote Blood Pressure Estimation via Narrow-band Multi-wavelength Pulse Transit Time', *ACM Trans. Sen. Netw.*, vol. 20, no. 4, pp. 1–21, Jul. 2024
[14] N. Ibtehaz *et al.*, 'PPG2ABP: Translating Photoplethysmogram (PPG) Signals to Arterial Blood Pressure (ABP) Waveforms', *Bioengineering*, vol. 9, no. 11, p. 692, Nov. 2022
[15] J. Park *et al.*, 'Photoplethysmogram Analysis and Applications: An Integrative Review', *Front. Physiol.*, vol. 12, p. 808451, Mar. 2022
[16] B.-J. Wu *et al.*, 'Camera-Based Blood Pressure Estimation via Windkessel Model and Waveform Features', *IEEE Trans. Instrum. Meas.*, vol. 72, pp. 1–13, 2023
[17] S. Hadiyoso *et al.*, 'Comparison of EMD, VMD and EEMD Methods in Respiration Wave Extraction Based on PPG Waves', *J. Phys.: Conf. Ser.*, vol. 1577, no. 1, p. 012040, Jul. 2020
[18] A. C. Yang *et al.*, 'Causal decomposition in the mutual causation system', *Nat Commun*, vol. 9, no. 1, p. 3378, Aug. 2018
[19] H.-C. Lee *et al.*, 'VitalDB, a high-fidelity multi-parameter vital signs database in surgical patients', *Sci Data*, vol. 9, no. 1, p. 279, Jun. 2022
[20] J. Proença *et al.*, 'Is pulse transit time a good indicator of blood pressure changes during short physical exercise in a young population?', in *2010 Annual International Conference of the IEEE Engineering in Medicine and Biology*, Buenos Aires, Argentina, Aug. 2010, pp. 598–601.
[21] J. Elith *et al.*, 'A working guide to boosted regression trees', *Journal of Animal Ecology*, vol. 77, no. 4, pp. 802–813, 2008
[22] R. Girshick, 'Fast R-CNN', presented at the Proceedings of the IEEE International Conference on Computer Vision, Santiago, Chile, 2015, pp. 1440–1448.
[23] E. O'Brien *et al.*, 'The British Hypertension Society protocol for the evaluation of automated and semi-automated blood pressure measuring devices with special reference to ambulatory systems', *Journal of Hypertension*, vol. 8, no. 7, pp. 607–619, 1990
[24] P. K. Whelton *et al.*, '2017 ACC/AHA/AAPA/ABC/ACPM/AGS/APhA/ASH/ASPC/NMA/PCNA Guideline for the Prevention, Detection, Evaluation, and Management of High Blood Pressure in Adults', *Journal of the American College of Cardiology*, vol. 71, no. 19, pp. e127–e248, May 2018
[25] L. Nilsson *et al.*, 'Respiratory variations in the photoplethysmographic waveform: acute hypovolaemia during spontaneous breathing is not detected', *Physiol. Meas.*, vol. 31, no. 7, pp. 953–962, Jul. 2010
[26] R. Mukkamala *et al.*, 'Toward Ubiquitous Blood Pressure Monitoring via Pulse Transit Time: Theory and Practice', *IEEE Trans. Biomed. Eng.*, vol. 62, no. 8, pp. 1879–1901, Aug. 2015
[27] L. Liu *et al.*, 'CiGNN: a causality-informed and graph neural network based framework for cuffless continuous blood pressure estimation', *IEEE Journal of Biomedical and Health Informatics*, vol. 28, no. 5, pp. 2674–2686, May 2024
[28] X. Song *et al.*, 'Causal Inference Based Hierarchical Regression Model for Cuffless Blood Pressure Estimation', in *2024 46th Annual International Conference of the IEEE Engineering in Medicine and Biology Society (EMBC)*, Orlando, FL, USA, Jul. 2024, pp. 1–4.
[29] Y. Wu *et al.*, 'Noninvasive Continuous Blood Pressure Measurement Method Based on EEMD and ANN', *Chinese Journal of Medical Instrumentation*, vol. 41, no. 4, pp. 235–239, 2017
[30] X. Song *et al.*, 'Combined forecast model of LSTM-CNN hypertension based on EEMD', in *2021 4th International Conference on Signal Processing and Machine Learning*, Beijing China, Aug. 2021, pp. 117–122.

Authorized licensed use limited to: Auckland University of Technology. Downloaded on November 25,2026 at 22:41:49 UTC from IEEE Xplore. Restrictions apply.
© 2026 IEEE. All rights reserved, including rights for text and data mining and training of artificial intelligence and similar technologies. Personal use is permitted, but republication/redistribution requires IEEE permission. See https://www.ieee.org/publications/rights/index.html for more information.